Structural evolution of layered $Li_{1.2}Ni_{0.2}Mn_{0.6}O_2$ upon electrochemical cycling in a Li rechargeable battery†

Jihyun Hong,[a] Dong-Hwa Seo,[a] Sung-Wook Kim,[a] Hyeokjo Gwon,[a] Song-Taek Oh[b] and Kisuk Kang*[a]

Received 22nd June 2010, Accepted 4th August 2010
DOI: 10.1039/c0jm01971b

Recently $Li_{1.2}Ni_{0.2}Mn_{0.6}O_2$, one of the most promising cathode candidates for next generation Li rechargeable batteries, has been consistently investigated especially because of its high lithium storage capacity, which exceeds beyond the theoretical capacity based on conventional chemical concepts. Yet the mechanism and the origin of the overcapacity have not been clearly understood. Previous reports on simultaneous oxygen evolution during the first delithiation may only explain the high capacity of the first charge process, and not of the subsequent cycles. In this work, we report a clarified interpretation of the structural evolution of $Li_{1.2}Ni_{0.2}Mn_{0.6}O_2$ upon the electrochemical cycling, which is the key element in understanding its anomalously high capacity, through careful study of electrochemical profiles, *ex situ* X-ray diffraction, HR-TEM, Raman spectroscopy, and first principles calculation. Moreover, we successfully resolved the intermediate states of structural evolution upon electrochemical cycles by intentionally synthesizing sample with large particle size. All observations made through various tools lead to the result that spinel-like cation arrangement and lithium environment are gradually created and locally embedded in layered framework during repeated electrochemical cycling. Moreover, through analyzing the intermediate states of the structural transformation, this gradual structural evolution could explain the mechanism of the continuous development of the electrochemical activity below 3.5 V and over 4.25 V.

Introduction

Rechargeable Li ion batteries power most of today's portable electronics. This is mainly due to their capability in offering the highest energy density compared to other battery technologies.[1–3] However, new fields of application for rechargeable Li ion batteries, such as hybrid electric vehicles (HEV), plug-in hybrid electric vehicles (PHEV), and electric vehicles (EV) and large scale power backups require the cathode materials, which are the key active component of the battery, to be improved in terms of energy/power density, cost, life time, and safety.[2,4–8] Intensive scientific research has been made in exploring new constituents that can substitute current commercial $LiCoO_2$ and $LiFePO_4$ electrode materials. Among them, the layered Li-excess nickel-manganese oxide ($Li[Li_{(1/3-2x/3)}Ni_xMn_{(2/3-x/3)}]O_2$, $0 < x < 1/2$, hereafter LLNMO), first introduced by Lu *et al.*,[9] manifests promising electrochemical properties with exceptionally high energy density.

It is believed that the abnormally high capacity is closely related to the initial structure of LLNMO and the structural change occurring during the cycles. LLNMO is a layered oxide compound composed of lithium layers fully filled with lithium ions and transition metal layers in which Ni and Mn ions coexist with excess Li ions. Theoretically,[10] as well as experimentally,[11–13] many researchers have confirmed the existence of Mn-rich regions and Li–Mn ordering in the structure of LLNMO. Furthermore, some researchers believe that this material is a nano-composite and should be written as $xLi_2MnO_3 \cdot (1-x)LiNi_{0.5}Mn_{0.5}O_2$ due to the Li–Mn ordering in the Mn-rich region and its corresponding peaks between 20–25° in X-ray diffraction patterns.[11,14] These peaks are reminiscent of Li_2MnO_3 with $C2/m$.

Generally Ni^{2+}/Ni^{4+} redox reaction is considered to be responsible for the reversible de-lithiation process, which contributes to the capacity, while Mn^{4+} ions stabilize the lattice framework in Ni–Mn based layered materials.[2,9,14–16] However, the specific capacity that is observed in LLNMO apparently far exceeds the corresponding theoretical capacity of the Ni^{2+}/Ni^{4+} redox couple.[9,17–20] The consequent uncertainty of the abnormally high capacity mechanism intrigued many researchers. As a result, they suggested several possibilities corresponding to this mechanism. Among them, Lu and Dahn suggested that both Li and O atoms were simultaneously removed to balance the charge neutrally during the first delithiation process.[18] Moreover Kim *et al.* also implied that the extraction of lithium was accompanied by oxygen loss during the first charging.[21] These findings were supported by Armstrong *et al.*'s observations of oxygen gas evolution from *in situ* mass spectroscopy analysis.[22]

Nevertheless, the oxygen evolution may only explain the first charge process; the high capacity at subsequent cycles should be elucidated further. Johnson *et al.* suggested the possibility that the origin of the abnormal capacity comes from the activation of the Li_2MnO_3 domain of the material, which leads the reduction of Mn^{4+} to a lower oxidation state.[23] However, there has been no

[a]*Department of Materials Science and Engineering/KAIST Institute for Eco-Energy, Korea Advanced Institute of Science and Technology (KAIST), 335 Gwahangno, Yuseong-gu, Daejeon, 305-701, Republic of Korea. E-mail: matlgen1@kaist.ac.kr*
[b]*LG Chem/Research Park, 104-1 Moonji-dong, Yuseong-gu, Daejeon, 305-380, Republic of Korea. E-mail: peacefulguy@lgchem.com*

† Electronic supplementary information (ESI) available: Comparison of the primary particle size of $Li_{1.2}Ni_{0.2}Mn_{0.6}O_2$ synthesized at 900 °C and 1000 °C using FE-SEM; cycle ability and Coulombic efficiency of $Li_{1.2}Ni_{0.2}Mn_{0.6}O_2$. See DOI: 10.1039/c0jm01971b

clear experimental evidence of reduction of Mn^{4+} yet. Even so Yoon *et al.* and Kang *et al.* showed that the transition metal reordering coincided with the disappearance of additional peaks between 20–25° after repeated electrochemical cycles through *in situ* and *ex situ* XRD analysis.[24,25] More recently, Jiang *et al.* also reported that the NMR signal from Li in $LiMn_6$ or $LiMn_5Ni$ environments gradually disappears with cycles.[12] In addition, Jiang *et al.* showed that cation migration happened at over 4.4 V, such that the Li vacancies in the transition metal layers are occupied by the other transition metal ions which can migrate from the adjacent sites through the solid-state NMR and TEM analysis.[12] Moreover, Tran *et al*. proposed that the formation of a perfect layered structure occurs with transition metals filling up Li vacancies in transition metal layers.[26] Despite these given pieces of information, it is not clear how the overall structural evolution of LLNMO occurs and to what structure it evolves.

All things considered, in this paper, we carefully investigate the structural evolution of $Li_{1.2}Ni_{0.2}Mn_{0.6}O_2$ ($Li[Li_{0.2}Ni_{0.2}Mn_{0.6}]O_2$, hereafter LL2NMO) during the electrochemical reaction using *ex situ* XRD, HR-TEM and Raman spectroscopy and first principles calculation. The creation of local spinel-like domains embedded in the original layered framework is observed. In order to carefully regard the intermediate states of structural evolution, we intentionally synthesized samples with large particle size (~1.2 μm). This process permitted the structural change from the electrochemical reaction to not occur too rapidly. Accordingly, we could investigate the gradual structural change as a function of cycles. In addition, the structural evolution at subsequent cycles (mainly cation rearrangement) could be successfully identified from the one at the first charge process (mainly oxygen evolution with Li extraction[18,21,22]).

Experimental details

Raw materials

Li_2CO_3 (99%), and $NaHCO_3$ (99%) were purchased from Junsei (Japan). $MnSO_4 \cdot H_2O$ (99%), $NiSO_4 \cdot 6H_2O$ (99%), LiOH (98%), and MnO_2 (99%) were purchased from Sigma–Aldrich (USA).

Sample preparation

The layered Li-excess nickel-manganese oxide (LL2NMO) was synthesized from mixed nickel-manganese carbonate precursors ($Ni_{0.25}Mn_{0.75}CO_3$) obtained *via* a co-precipitation method. A 0.2 M mixed $NiSO_4$ and $MnSO_4$ aqueous solution (Ni : Mn = 1 : 3) was added drop-wise to an equal volume of a 1 M $NaHCO_3$ aqueous solution under constant stirring of 250 rpm at 50 °C. The pH was maintained at 8 by adding ammonium hydroxide. The mixed solution containing green precipitates that are formed immediately, was aged for 24 h under the same conditions of the co-precipitation procedure. The $Ni_{0.25}Mn_{0.75}CO_3$precipitate was filtered, washed with deionized water several times, and dried overnight at 120 °C. The dried powder was mixed with a 5% excess of stoichiometric amount of Li_2CO_3 to compensate for possible lithium loss during the calcination. The mixture was heated at 1000 °C for 6 h in air then quenched to room temperature using two copper plates. The spinel lithium manganese oxide ($LiMn_2O_4$) was synthesized by the solid-state method. The mixture of LiOH and MnO_2 (Li : Mn = 1 : 2) was heated in air first at 750 °C for 4 h, then ground, and eventually they were reheated again for 12 h at 750 °C.[27]

Compound confirmation

The crystal structure of the various compounds synthesized were characterized using a D/MAX-RB powder X-ray diffractometer (Rigaku, Japan) equipped with Cu-Kα radiation ($\lambda = 1.54178$ Å) with scanning speed of 1° min^{-1} in the 2θ range of 10–75°. The stoichiometry of the synthesized compound was determined by inductively coupled plasma atomic emission spectroscopy (ICP-AES, Thermo Jarrel Ash, Polyscan 60E, USA). The size and morphology of the particles were measured using a field emission scanning electron microscope (FE-SEM, Philips, XL30 FEG, Netherlands).

Electrochemical analysis

Tested electrodes were fabricated by the following sequences. A slurry of 84 wt% $Li_{1.2}Ni_{0.2}Mn_{0.6}O_2$, 4 wt% carbon black (Super-P, TIMCAL), 4 wt% graphite (SFG-6, TIMCAL), and 8 wt% polyvinylidene fluoride (PVDF) binder dissolved in N-methyl-1,2-pyrrolidone (NMP, Sigma-Aldrich, 99.5%) was cast onto aluminium foils using a doctor-blade. NMP was evaporated at 120 °C for 2 h. Coin cells (CR2016, Hohsen, Japan) were assembled with the $Li_{1.2}Ni_{0.2}Mn_{0.6}O_2$ electrode, the Li counter electrode, a separator (Celgard 2400), and a 1 M solution of $LiPF_6$ in a mixture of ethyl carbonate/dimethyl carbonate (EC/DMC, 1 : 1 v/v) in an argon-filled glove box. The galvanostatic charge/discharge profile was measured at a voltage range of 2.0–4.8 V by a potentio-galvanostat (WonA Tech, WBCS 3000, Korea) at 16 mA g^{-1}, at room temperature for 40 cycles.

Ex situ structural analysis

Several electrodes after various numbers of cycles (as-prepared, 1 cycle, 2 cycles, 5 cycles, 10 cycles, 20 cycles, and 40 cycles) were selected to observe the gradual structural evolution. The electrodes fully discharged to 2.0 V were disassembled from coin cells and rinsed with dimethyl carbonate several times and dried at room temperature. For high resolution transmission electron microscope (HR-TEM) analysis, the active material were raked out and dispersed in NMP. Then they were transferred onto carbon coated Cu grids for further analysis. HR-TEM images of the samples were recorded using a field emission transmission electron microscope (FE-TEM, Jeol, JEM-2100F, Japan). Lattice parameters were determined by the Rietveld refinements using the Fullprof software.[28] The local structural evolution of the LL2NMO compound during electrochemical cycling was confirmed and identified by a high resolution dispersive Raman microscope (Horiban Jobin Yvon, LabRAM HR UV/Vis/NIR, France) equipped with argon ion CW laser ($\lambda = 514.5$ nm) at room temperature. The local vibrations of the spinel $LiMn_2O_4$ polycrystalline electrode samples and those electrochemically discharged to 2.0 V ($Li_{(1+x)}Mn_2O_4$) were measured for the comparison.

Calculation details

First principles calculation was done with the spin-polarized generalized gradient approximation (GGA). As implemented in the Vienna *ab initio* simulation package (VASP),[29] it uses the Perdew–Burke–Ernzerhof exchange–correlation parametrization[30] to density functional theory (DFT), applying a plane-wave basis set and the projector-augmented wave (PAW) method. PAW potentials have been widely used for battery materials and they have shown good predictive capability.[2] A plane-wave basis with a kinetic energy cutoff of 400 eV was used, and appropriate k-point meshes were chosen to ensure that the total energies are converged within 1 meV per formula unit. All the layered $LiMnO_2$, $LiNiO_2$, and the over lithiated spinel $Li_2Mn_2O_4$, $Li_2Ni_2O_4$ structures were fully relaxed to obtain the lattice parameters.

Results and discussion

Structural confirmation of as-prepared $Li_{1.2}Ni_{0.2}Mn_{0.6}O_2$

The crystal structure of the synthesized LL2NMO was investigated by XRD as shown in Fig. 1. It shows the typical diffraction pattern of LLNMO layered materials. Every peak except for those between 20–25° agrees well with the $R\bar{3}m$ space group of the α-$NaFeO_2$ structure. The clear peak separations at 37° ((006) *vs.* (012)) and 65° ((018) *vs.* (110)) signify that this material constitutes a well crystallized layered structure without spinel structure.[17] Peaks present between 20–25° that can be indexed with lower symmetry $C2/m$ space group indicate the presence of $LiMn_6$ or $LiMn_5Ni$ super-structures in the transition metal layers, or local Li_2MnO_3-like structure created due to electrostatic interaction between cations.[10–12,17] The exact composition of the as-prepared compound measured by ICP-AES was $Li_{1.234}Ni_{0.186}Mn_{0.582}O_2$. This complies well with the target composition.

Fig. 2 shows typical morphologies and sizes of the as-prepared particles observed by FE-SEM. The size of the primary particles is approximately 0.6–1.2 μm, which is much larger than the values reported by others[31,32] as well as particles synthesized at 900 °C as shown in S1†. These intentionally enlarged particles would experience structural evolution much more slowly over several electrochemical cycles as described later.[33] All in all, it allows us to trace the intermediate structures and the tendency of structural evolution. However, as Dahn *et al.* reported,[34] LL2NMO synthesized at both 900 °C and 1000 °C have almost identical properties except that the sample heated at higher temperature is relatively well crystallized.

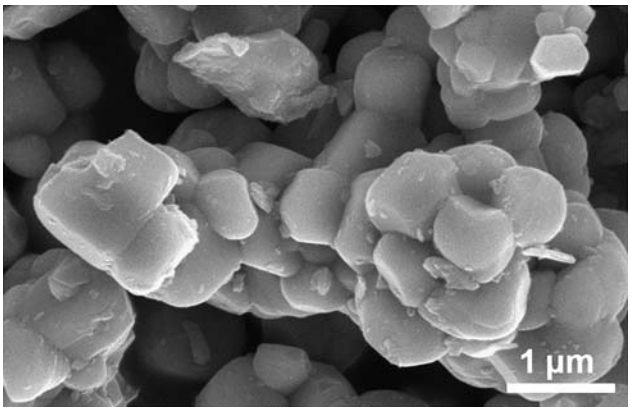

Fig. 2 Morphology of the as-prepared particles observed by FE-SEM. The size of the primary particles is about 600 nm–1.2 μm which is much larger than those of the sample synthesized at 900 °C (300–400 nm), as shown in S1†.

Gradual structural evolution of $Li_{1.2}Ni_{0.2}Mn_{0.6}O_2$ upon electrochemical cycling

The electrochemical activity of LL2NMO electrode *vs.* Li is measured at 16 mA g^{-1} for 40 cycles at room temperature. Its charge–discharge profiles at the 1st, 2nd, 5th, 10th, 20th and 40th cycles are shown in Fig. 3. As reported previously, there is a plateau near 4.5 V at the first charge, which may correspond to the simultaneous oxygen release with lithium deintercalation

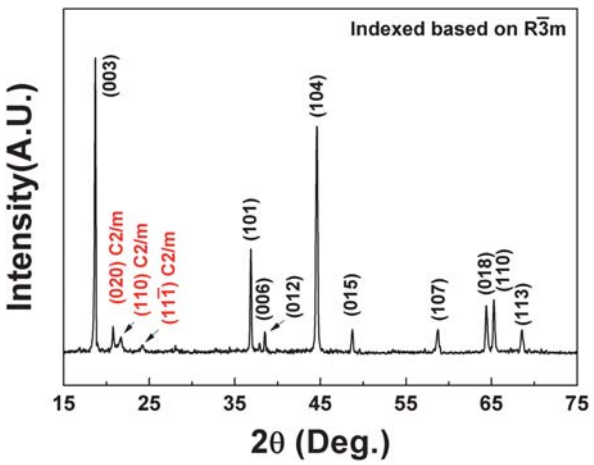

Fig. 1 XRD pattern of the $Li_{1.2}Ni_{0.2}Mn_{0.6}O_2$ indexed based on the $R\bar{3}m$ structure. The peaks between 20 and 25° corresponding to Li–Mn ordering in transition metal layers can be indexed with the $C2/m$ structure.

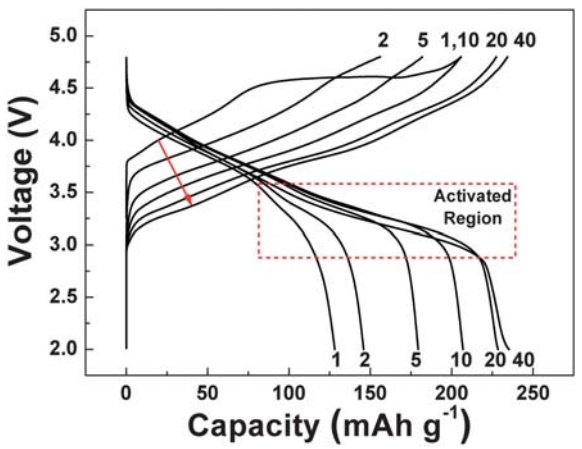

Fig. 3 Charge–discharge profiles of $Li_{1.2}Ni_{0.2}Mn_{0.6}O_2$ electrode *vs.* Li at 16 mA g^{-1} at the 1st, 2nd, 5th, 10th, 20th, and 40th cycle. The electrochemical activity below 3.5 V gradually develops both in charge and discharge as number of cycles increases.

($LiMO_2 \rightarrow Li_{(1-2x)}MO_{(2-x)} + 2x\ Li + x/2\ O_2\uparrow$, M = Ni, Mn, Li).[18,20,21] However, there is a remarkable change in the profile with cycles.

The most significant change is that the electrochemical activity below 3.5 V gradually develops both in charge and discharge following the 40th cycle. The activation of Li de/intercalation between 3.5 V and 3.0 V considerably contributes to the increase of overall capacity. The capacity over 3.5 V also slightly increases with the activation of reaction over 4.25 V for extended cycles. Consequently, the overall capacity gradually increases from 128 mAh g^{-1} in the first cycle to 238 mAh g^{-1} in the 40th cycle. After the 20th cycle, the capacity from the reaction over 3.5 V slowly decays, while the electrochemical activity below 3.5 V still slightly increases. The capacity from the reaction below 3.5 V and over 4.25 V continues to increase implying that the repeated electrochemical cycling activates the Li de/intercalation process at this potential range. Apparently, the change of the profile does not result from the polarization, which is often observed during the battery cycling. This can be proven by the shift of the average value of charge and discharge voltages determined thermodynamically.

The differential capacity curve (dQ/dV *vs.* V) of the 1st, 5th, 10th, 20th, and 40th discharge was also plotted for more careful analysis of electrochemical profile, as shown in Fig. 4a. It is easily identified that most reaction occurs at near 4 V with only a slight peak near 3.25 V at the first discharge. The width and the height of the peak at 4 V slightly increased over the 20 cycles with the appearance of a new reaction at about 4.25 V. After the 20th cycle, the area of the peak at 4.25 V still remains almost the same. As the number of cycles increases, the peak near 3.25 V grows significantly and slightly shifts to a lower voltage range near 3 V, indicating new electrochemical reactions at these voltage ranges. For comparison, the dQ/dV curve of the charge process was plotted for the 2nd, 5th, 10th, 20th, and 40th charge cycles in Fig. 4b. In a good agreement with the discharge process, the electrochemical activity below 3.5 V is also significantly enhanced in the charge process implying that the change in the discharge profile is not of a purely kinetic but thermodynamic nature. Because reaction voltage is determined by lithium chemical potential ($V(x) = (\mu^{Li}_{cathode} - \mu^{0}_{anode})/zF$),[35] the activation indicates that the host structure of Li continuously changes during the electrochemical processes. The appearance of the reaction at different voltage ranges signifies the formation of a structure with different lithium environments where lithium ions have different chemical potentials.

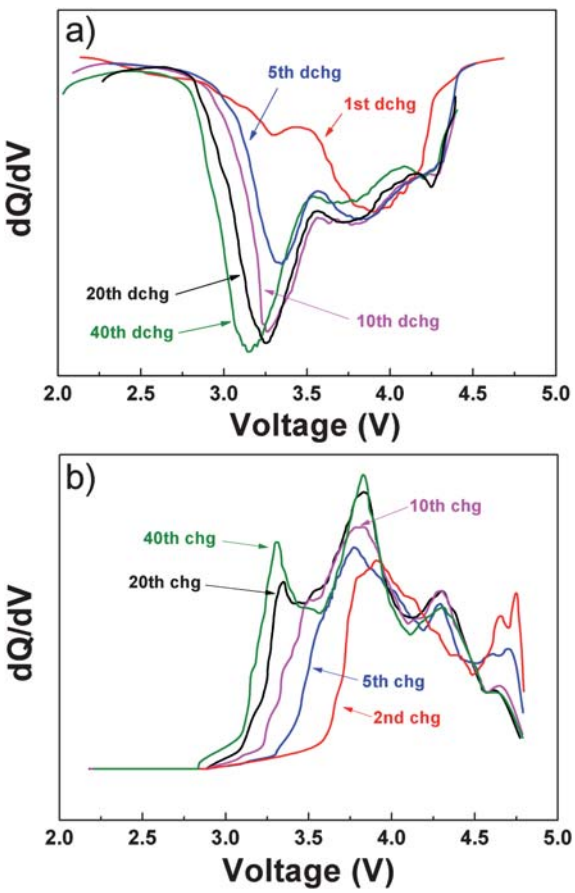

Fig. 4 Differential capacity curves of a) the 1st, 5th, 10th, 20th, and 40th discharge and b) the 2nd, 5th, 10th, 20th, and 40th charge at 16 mA g^{-1}. The peak near 3.25 V grows significantly and slightly shifts to lower voltage range near 3.15 V. A new narrow peak at about 4.25 V emerges as cycle continues indicating a new electrochemical reaction at this voltage.

It should be noted that, even after the first charge, the structure continues to change without an apparent plateau at around 4.5 V which is indicative of oxygen evolution.[22] Moreover, electrochemical activity below 3.5 V continuously develops without a large capacity increase over 3.5 V after the 10th cycle. This may imply that the structural evolution during subsequent cycles does not necessarily accompany simultaneous oxygen evolution. From the fact that there is no apparent 4.5 V plateau at subsequent cycles, it can be speculated that the structural evolution, which activates the potential region below 3.5 V, is mainly related to the atomic rearrangement in the crystal after oxygen evolution. It is noteworthy that the full activation below 3.5 V takes some time even after the loss of oxygen from the structure.

Creation of local spinel-like cation arrangements in the layered framework

The confirmation of the structural evolution during the battery cycling was performed with *ex situ* XRD analysis, as shown in Fig. 5. The fully lithiated electrodes after the 1st, 2nd, 5th, 10th, 20th, and 40th cycle were investigated under XRD. As reported previously by others, the series of peaks between 20–25°, related to Li_2MnO_3-like structures, considerably broaden after the first two cycles. Moreover, they finally disappear after the 5th cycle.[12,25] This indicates that Li–Mn ordering has been removed in the transition metal layers and cannot be recovered on discharge. This implies that atomic rearrangement definitely occurs during the electrochemical cycling, and the crystal structure of the material does not return to the original state. In addition, we observed that XRD peaks continuously shift to the lower 2θ angle as the electrochemical cycling repeats. The exact changes of lattice parameters *a* and *c* were quantitatively confirmed by the Rietveld refinements of XRD patterns. Fig. 6 shows the calculated lattice parameters of samples at various cycles. Both lattice parameters *a* and *c* continuously increase during the electrochemical tests (*a*: 2.8544 to 2.8859 Å, *c*: 14.2483 to 14.4472 Å). Especially, the increase of lattice parameters in the

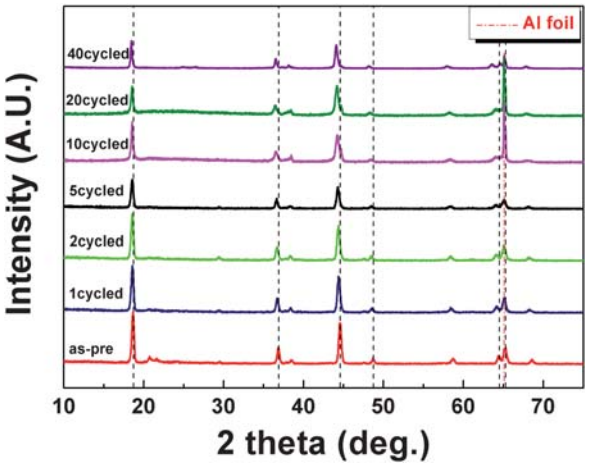

Fig. 5 *Ex situ* XRD patterns of as-prepared material and the electrodes after 1st, 2nd, 5th, 10th, 20th, and 40th cycle. The peaks continuously shift to the lower 2θ angle as the electrochemical cycling repeats.

initial few cycles is rapid, but eventually it slows down. This represents clear evidence that, in our sample, the structural evolution proceeds through the cycles. Lattice expansion along both *a* and *c* axes are rather abnormal phenomena in the layered structures. Generally at near fully lithiated states, *c* lattice parameter can increase with slight delithiation resulting from the electrostatic repulsion across the Van der Waals gap between the transition metal oxide sheets. However, in the same case lattice parameter *a* typically decreases because the size of transition metal ion reduces as a result of the oxidation of valence state.[36] Hence, the increase in both lattice parameters indicates that the augment does not develop from artifacts such as slight lithium composition change, but from atomic rearrangements in the crystal structure.

In order to have detailed information on the structural evolution, HR-TEM analysis was performed. Fig. 7 shows HR-TEM images of a) as-prepared LL2NMO and b) and c) electrode after 40 electrochemical cycles. Parallel lattice in Fig. 7a corresponds to the typical layered materials with interplanar distances of about 4.7 Å which corresponds to the distances of the close-packed (003) planes of the $R\bar{3}m$ layered structure (or (001) planes of $C2/m$). This parallel lattice was observed over whole region of the material, which means that the pure single layered structured phase was built up throughout the as-prepared LL2NMO. In the HR-TEM image of the fully activated material after 40 electrochemical cycles, unexpectedly, particular patterns in lattices were observed which were different from the as-prepared material. In Fig. 7b and 7c, reticulate patterns are detected locally in original

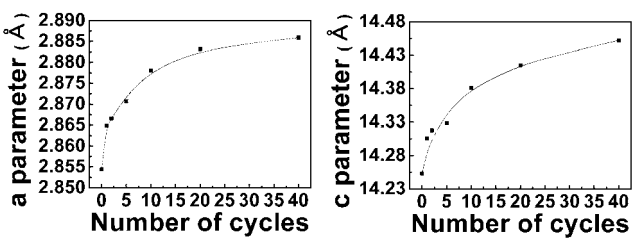

Fig. 6 Lattice parameters *a* and *c* of the $R\bar{3}m$ structure measured by the Rietveld refinements. Both *a* and *c* increase with the number of cycles.

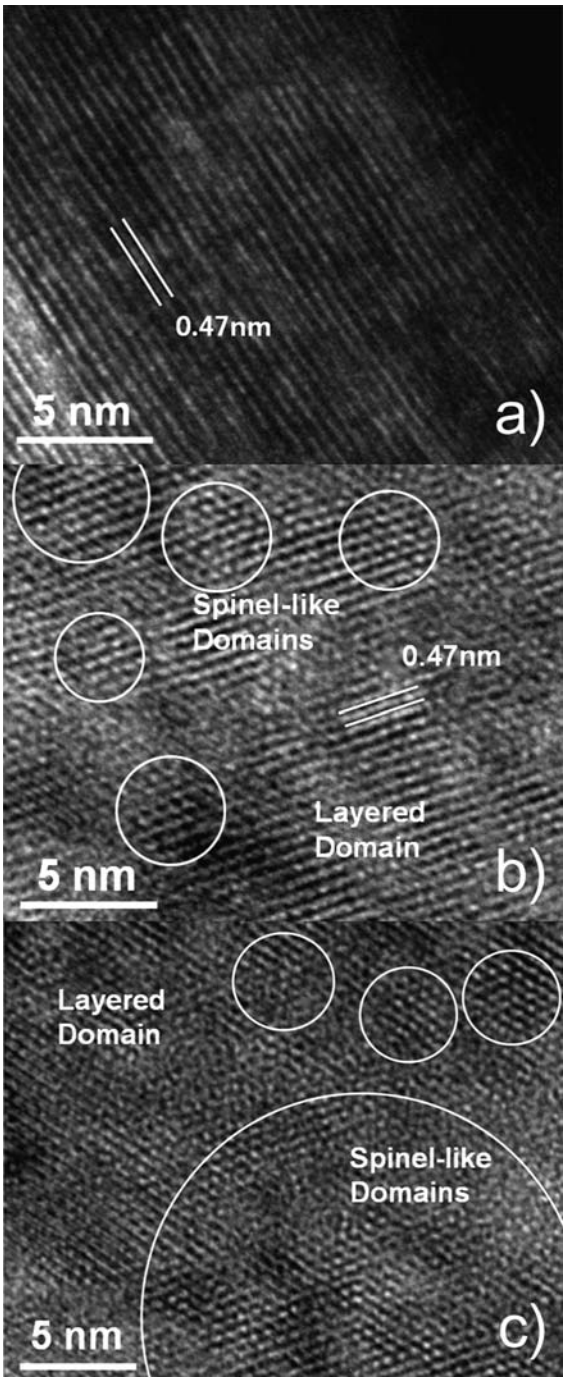

Fig. 7 HR-TEM image of a) as-prepared LL2NMO and b) and c) the material after 40 electrochemical cycles. a) Parallel lines are comparable to those of (003) planes of the layered structure with interplanar distance of approximately 4.7 Å. b) and c) Highlighted circles indicate the local structure of spinel-like domain with reticulate lattice embedded in the original layered framework which resulted from the structural evolution.

parallel lines which seem to be the remarkable topotactic characteristics of the (111) planes of spinel phases, distinguishable from the layered structure to which the close-packed (003) planes of layered component are aligned parallel.[11,23] This strongly indicates that the cation ordering in the layered structure has locally changed into spinel-like phase which contains transition

metal ions in both lithium layers and transition metal layers. A number of this kind of spinel-like nano-sized domains were found at various sections of the sample. However, the creation of the spinel-like cation ordering did not destroy the original layered structure and is locally embedded into the layered framework over the entirety of the particles.

In order to confirm the newly created local spinel-like cation rearrangement, a micro Raman spectroscopic study of the sample was performed. Raman spectroscopy has been proven to be useful in exhibiting the difference between various structures of different atomic orderings.[37–39] It has been especially proven to be extremely sensitive to local bonding changes from layered to spinel structure.[40,41] Fig. 8a shows Raman spectra of the as-prepared LL2NMO and the electrode after 5 and 40 electrochemical cycles. For comparison, Raman spectra from $LiMn_2O_4$ and electrochemically lithiated spinel $Li_{(1+x)}Mn_2O_4$ are measured and shown in Fig. 8b. The Raman spectrum of the as-prepared compound contains three peaks near 603 cm^{-1}, 485 cm^{-1}, and 428 cm^{-1}. In general, there exist two Raman-active vibrational modes in layered lithium transition metal oxide with $R\bar{3}m$ symmetry. They have been described as A_{1g} with the symmetrical stretching of M–O, and E_g with the symmetrical deformation.[42] Two peaks near 603 cm^{-1} and 485 cm^{-1} of the as-prepared material in the figure are assigned as A_{1g} and E_g respectively. An additional small peak at 428 cm^{-1} originated from the Li_2MnO_3-like structure of the Mn-rich region due to the reduced local symmetry of $C2/m$ rather than $R\bar{3}m$.[43] The A_{1g} peak (603 cm^{-1}) is relatively sharp without any splits which means that the Li_2MnO_3-like Mn-rich region is well mixed with the $LiMO_2$ region (here, $LiNi_{(0.5\pm x)}Mn_{(0.5\pm x)}O_2$) in as-prepared LL2NMO. However, these patterns are significantly altered in the sample after 5 cycles and 40 cycles. After 5 electrochemical cycles, the A_{1g} peak begins to be divided into two different A_{1g} peaks at about 600 cm^{-1} and 625 cm^{-1}. In the fully activated 40 cycled sample, the separation of A_{1g} is much clearer. Raman spectra of the sample after 40 electrochemical cycles show a strong peak at 625 cm^{-1} with a big shoulder peak at around 585 cm^{-1} and two other peaks at 485 cm^{-1} and 375 cm^{-1}. The sharp distinction of two A_{1g} peaks signifies the existence of two different local M–O arrangements. The electrochemical activity development below 3.5 V in Fig. 4 is accompanied by the A_{1g} peak division.

This is reminiscent of mixed characteristics of both spinel and layered phases. Typical Raman spectra of $LiMn_2O_4$ with $Fd\bar{3}m$ symmetry show a strong A_{1g} peak at around 630 cm^{-1}, whose position is characteristic of cubic spinel, distinguishable from the layered phase which exhibits three small peaks around 585 cm^{-1}, 474 cm^{-1}, and 375 cm^{-1}.[40,44–46] A peak near 375 cm^{-1}, which can be assigned as F_{2g}, is known to correspond to the symmetrical stretching mode of LiO_4 tetrahedra.[47] When the spinel $LiMn_2O_4$ is discharged to 2.0 V, the A_{1g} peak slightly shifts to the left and is located at 625 cm^{-1}, as shown in Fig. 8b. The two peaks at 625 cm^{-1} and 375 cm^{-1} in the 40 cycled sample are the strong indication of the existence of spinel-like cation ordering. On the other hand, the big shoulder peak near 585 cm^{-1} and the peak at 485 cm^{-1} imply that the layered characteristic of the $LiMO_2$ (M = Ni, Mn) domain are present in the sample.[48,49] This mixed behavior is in very good agreement with the observation drawn from the HR-TEM images, which confirmed that the local spinel-like ordering is embedded in the layered framework. A peak at 428 cm^{-1} of the as-prepared material is unidentified in the sample after 40 cycles. This indicates that the Li_2MnO_3-like ordering is lost after the battery cycling, which also agrees well with the *ex situ* XRD results.

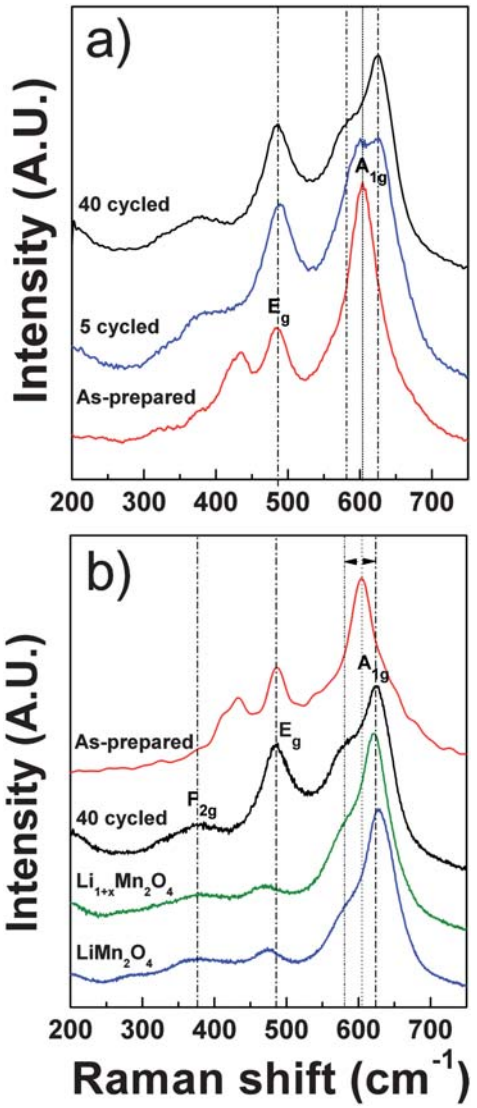

Fig. 8 Raman spectra of a) the as-prepared electrode, electrode after 5 cycles, and electrode after 40 cycles, b) as-prepared electrode, electrode after 40 cycles, spinel $LiMn_2O_4$, and lithiated spinel $Li_{(1+x)}Mn_2O_4$. The A_{1g} peak of as-prepared material splits into two different peaks upon electrochemical cycling. The Raman spectrum of the 40 cycled sample is reminiscent of mixed characteristics of both spinel and layered phases implying that the final structure contains local spinel-like cation ordering in the original layered structure.

In the event of a local transformation into a spinel-like structure, it is expected that Li de/intercalation should occur at a different potential than in the original layered structure. The reactions appearing near 4.25 V and below 3.5 V observed in Fig. 4 are likely to be related to this transformation. It should be noted that the Mn^{3+}/Mn^{4+} redox reaction occurs near 4.25 V in the nickel doped spinel lithium manganese oxide when the atomic ratio of Ni to Mn is less than 1/3.[50] The activation of the

Li_2MnO_3 region in LL2NMO seems to be a consequence of this structural evolution.

In order to link the appearance of spinel-like ordering with the increase of the lattice parameters during the cycles observed in the *ex situ* XRD study, we used the following method; the general trend of lattice parameters, of when transformation occurs from the layered to the spinel in layered oxygen framework, was investigated by first principles calculation. It was observed that calculated lattice parameters of spinel cation ordering are consistently bigger in both *a* and *c* axes than those of layered cation ordering in layered oxygen framework, as shown in Table 1, for four different simplified lithium transition metal oxides (layered $LiNiO_2$, $LiMnO_2$ and lithiated spinel $Li_2Ni_2O_4$, $Li_2Mn_2O_4$). This explains why the *a* and *c* lattice parameters should increase when there is a partial spinel-like transformation in the layered framework. The increase of the values is consistent with the observation in *ex situ* XRD analysis. It is important to mention that *c*/*a* ratio does not change significantly from the layered to spinel for $LiMnO_2$ in contrast to the case of $LiNiO_2$. In fact, the *c*/*a* ratio of LL2NMO does not significantly change even after 40th cycle. This result reflects that the Mn-rich region is likely to be more responsible for the structural evolution of this material.

Conclusions

In this study, we investigated the structural evolution of $Li_{1.2}Ni_{0.2}Mn_{0.6}O_2$ upon repeated electrochemical cycling through careful analysis of electrochemical profiles, *ex situ* XRD, HR-TEM, Raman spectroscopy, and first principles calculations. The observations made in this report all lead to a conclusion that the originally well mixed layered LL2NMO slowly evolves to a nano-composite structure where spinel-like regions are locally embedded in the layered $LiMO_2$ framework. Moreover, by analyzing the intermediate states of the structural transformation, we concluded that this gradual structural evolution could explain the mechanism of the continuous development of the electrochemical activity below 3.5 V and over 4.25 V.

In fact, this kind of structural transformation is not unnatural. While Mn composition over Ni in LL2NMO is about 3 : 1, there may be regions where Mn contents are high enough to be denoted as $Li_{(1+x)}Mn_{(1-x)}O_2$. The locally distributed layered lithium manganese oxide phases are naturally subject to structural evolution to spinel phases during the electrochemical cycling as reported by other senior scientists.[3,51,52]

Table 1 Calculated and measured lattice parameters of layered and spinel structures based on layered oxygen framework. In the case of the spinel structure, lattice parameter *a* is the distance between two adjacent transition metals in the same layer, and *c* is the sum of the three interplanar distances perpendicular to *a*

	Lattice parameter *a*	Lattice parameter *c*	Ratio *c*/*a*
Layered $LiMnO_2$	2.815	14.027	4.983
Spinel $Li_2Mn_2O_4$	2.930	14.546	4.965
Layered $LiNiO_2$	2.861	13.769	4.813
Spinel $Li_2Ni_2O_4$	2.867	14.135	4.930
$Li_{1.2}Ni_{0.2}Mn_{0.6}O_2$[a]	2.8544	14.2483	4.992
Cycled $Li_{1.2}Ni_{0.2}Mn_{0.6}O_2$[a]	2.8859	14.4472	5.006

[a] Measured by Rietveld refinements.

Acknowledgements

This work was supported by Energy Resources Technology R&D program (20092020100040) under the Ministry of Knowledge Economy, Republic of Korea. This research was supported by the National Research Foundation of Korea Grant funded by the Korean Government (MEST) (NRF-2009-0094219). This research was supported by the Korea Science and Engineering Foundation (KOSEF) grant funded by the Korea government (MEST) (R11-2008-058-01003-0). This research was supported by the Converging Research Center Program through the National Research Foundation of Korea (NRF) funded by the Ministry of Education, Science and Technology (No. 2009-0082069). The authors are grateful to Kisti (Grant No. KSC-2009-S03-0011) for providing supercomputing resources.

Notes and references

1 M. Winter and R. J. Brodd, *Chem. Rev.*, 2004, **104**, 4245–4270.
2 K. Kang, Y. S. Meng, J. Breger, C. P. Grey and G. Ceder, *Science*, 2006, **311**, 977–980.
3 A. R. Armstrong and P. G. Bruce, *Nature*, 1996, **381**, 499–500.
4 Y. J. Lee, H. Yi, W. J. Kim, K. Kang, D. S. Yun, M. S. Strano, G. Ceder and A. M. Belcher, *Science*, 2009, **324**, 1051–1055.
5 M. Armand and J. M. Tarascon, *Nature*, 2008, **451**, 652–657.
6 M. S. Whittingham, *Science*, 1976, **192**, 1126–1127.
7 D. H. Seo, H. Gwon, S. W. Kim, J. Kim and K. Kang, *Chem. Mater.*, 2010, **22**, 518–523.
8 H. Gwon, D.-H. Seo, S.-W. Kim, J. Kim and K. Kang, *Adv. Funct. Mater.*, 2009, **19**, 3285–3292.
9 Z. H. Lu, D. D. MacNeil and J. R. Dahn, *Electrochem. Solid-State Lett.*, 2001, **4**, A191–A194.
10 A. Van der Ven and G. Ceder, *Electrochem. Commun.*, 2004, **6**, 1045–1050.
11 M. M. Thackeray, C. S. Johnson, J. T. Vaughey, N. Li and S. A. Hackney, *J. Mater. Chem.*, 2005, **15**, 2257–2267.
12 M. Jiang, B. Key, Y. S. Meng and C. P. Grey, *Chem. Mater.*, 2009, **21**, 2733–2745.
13 S. H. Kang, P. Kempgens, S. Greenbaum, A. J. Kropf, K. Amine and M. M. Thackeray, *J. Mater. Chem.*, 2007, **17**, 2069–2077.
14 M. M. Thackeray, S. H. Kang, C. S. Johnson, J. T. Vaughey, R. Benedek and S. A. Hackney, *J. Mater. Chem.*, 2007, **17**, 3112–3125.
15 J. Reed and G. Ceder, *Electrochem. Solid-State Lett.*, 2002, **5**, A145–A148.
16 T. Ohzuku and Y. Makimura, *Chem. Lett.*, 2001, 744–745.
17 Z. H. Lu, L. Y. Beaulieu, R. A. Donaberger, C. L. Thomas and J. R. Dahn, *J. Electrochem. Soc.*, 2002, **149**, A778–A791.
18 Z. H. Lu and J. R. Dahn, *J. Electrochem. Soc.*, 2002, **149**, A815–A822.
19 J. S. Kim, C. S. Johnson and M. M. Thackeray, *Electrochem. Commun.*, 2002, **4**, 205–209.
20 A. D. Robertson and P. G. Bruce, *Chem. Mater.*, 2003, **15**, 1984–1992.
21 J. S. Kim, C. S. Johnson, J. T. Vaughey, M. M. Thackeray and S. A. Hackney, *Chem. Mater.*, 2004, **16**, 1996–2006.
22 A. R. Armstrong, M. Holzapfel, P. Novak, C. S. Johnson, S. H. Kang, M. M. Thackeray and P. G. Bruce, *J. Am. Chem. Soc.*, 2006, **128**, 8694–8698.
23 C. S. Johnson, J. S. Kim, C. Lefief, N. Li, J. T. Vaughey and M. M. Thackeray, *Electrochem. Commun.*, 2004, **6**, 1085–1091.
24 W. S. Yoon, N. Kim, X. Q. Yang, J. McBreen and C. P. Grey, *J. Power Sources*, 2003, **119**, 649–653.
25 S. H. Kang, Y. K. Sun and K. Amine, *Electrochem. Solid-State Lett.*, 2003, **6**, A183–A186.
26 N. Tran, L. Croguennec, M. Menetrier, F. Weill, P. Biensan, C. Jordy and C. Delmas, *Chem. Mater.*, 2008, **20**, 4815–4825.
27 Q. M. Zhong, A. Bonakdarpour, M. J. Zhang, Y. Gao and J. R. Dahn, *J. Electrochem. Soc.*, 1997, **144**, 205–213.
28 T. Roisnel and J. Rodríquez-Carvajal, *Mater. Sci. Forum*, 2001, 118–123.

29 G. Kresse and J. Furthmuller, *Comput. Mater. Sci.*, 1996, **6**, 15–50.
30 J. P. Perdew, K. Burke and M. Ernzerhof, *Phys. Rev. Lett.*, 1996, **77**, 3865–3868.
31 Y. J. Kang, J. H. Kim, S. W. Lee and Y. K. Sun, *Electrochim. Acta*, 2005, **50**, 4784–4791.
32 H. X. Deng, I. Belharouak, Y. K. Sun and K. Amine, *J. Mater. Chem.*, 2009, **19**, 4510–4516.
33 A. Van Bommel and J. R. Dahn, *ECS Meeting Abstracts*, 2009, **902**, 426–426.
34 Z. H. Lu, Z. H. Chen and J. R. Dahn, *Chem. Mater.*, 2003, **15**, 3214–3220.
35 M. K. Aydinol, A. F. Kohan and G. Ceder, *J. Power Sources*, 1997, **68**, 664–668.
36 J. Choi and A. Manthiram, *J. Electrochem. Soc.*, 2005, **152**, A1714–A1718.
37 M. Delhaye and P. Dhamelincourt, *J. Raman Spectrosc.*, 1975, **3**, 33–43.
38 M. Delhaye, M. Bridoux and F. Wallart, *J. Mol. Struct.*, 1982, **79**, 51–66.
39 S. Loridant, L. Abello, E. Siebert and G. Lucazeau, *Solid State Ionics*, 1995, **78**, 249–258.
40 S. J. Hwang, H. S. Park, J. H. Choy, G. Campet, J. Portier, C. W. Kwon and J. Etourneau, *Electrochem. Solid-State Lett.*, 2001, **4**, A213–A216.
41 C. M. Julien and M. Massot, *Mater. Sci. Eng., B*, 2003, **100**, 69–78.
42 W. W. Huang and R. Frech, *Solid State Ionics*, 1996, **86–8**, 395–400.
43 S. K. Jeong, C. H. Song, K. S. Nahm and A. M. Stephan, *Electrochim. Acta*, 2006, **52**, 885–891.
44 B. Ammundsen, G. R. Burns, M. S. Islam, H. Kanoh and J. Roziere, *J. Phys. Chem. B*, 1999, **103**, 5175–5180.
45 W. W. Huang and R. Frech, *J. Power Sources*, 1999, **81**, 616–620.
46 H. Kanoh, W. P. Tang and K. Ooi, *Electrochem. Solid-State Lett.*, 1998, **1**, 17–19.
47 C. M. Julien and M. Massot, *Mater. Sci. Eng., B*, 2003, **97**, 217–230.
48 H. Xia, L. Lu and Y. S. Meng, *Appl. Phys. Lett.*, 2008, **92**, 3.
49 H. Xia, Y. S. Meng, M. O. Lai and L. Lu, *J. Electrochem. Soc.*, 2010, **157**, A348–A354.
50 S. Patoux, L. Daniel, C. Bourbon, H. Lignier, C. Pagano, F. Le Cras, S. Jouanneau and S. Martinet, *J. Power Sources*, 2009, **189**, 344–352.
51 A. R. Armstrong, N. Dupre, A. J. Paterson, C. P. Grey and P. G. Bruce, *Chem. Mater.*, 2004, **16**, 3106–3118.
52 J. Reed, G. Ceder and A. Van der Ven, *Electrochem. Solid-State Lett.*, 2001, **4**, A78–A81.

